

# Effect of helium ion irradiation on pure W, W-5Ta and W-5Re: a micro-tensile and nanoindentation investigation of mechanical properties

Alan Xu<sup>1,2,\*</sup>, Tao Wei<sup>1</sup>, Ken Short<sup>1</sup>, Tim Palmer<sup>1</sup>, Mihail Ionescu<sup>1</sup>, Dhriti Bhattacharyya<sup>1,2</sup>, George D. W. Smith<sup>3</sup>, David E.J. Armstrong<sup>3</sup>

<sup>1</sup> Nuclear Fuel Cycle Research, Australian Nuclear Science and Technology Organisation, New Illawarra Road, Lucas Heights, New South Wales, 2234, Australia,

<sup>2</sup> School of Materials Science and Engineering, University of New South Wales, Sydney, New South Wales, 2052, Australia

<sup>3</sup> University of Oxford, Department of Materials, Parks Road, Oxford OX1 3PH, UK

\* corresponding author: [alan.xu@ansto.gov.au](mailto:alan.xu@ansto.gov.au)

## Abstract

Micro-tensile testing has been used to study the response of pure tungsten and two tungsten alloys to helium ion irradiation. Commercially supplied plates of W, W-5Ta and W-5Re were irradiated using 6MeV helium ions at room temperature. The ion energy was attenuated with an energy spreading device such that a uniform level of damage at 0.6 dpa (and 11,000 appm He) was deposited at the 3 – 9  $\mu\text{m}$  depth. Focused ion beam milling was used to fabricate dog-bone shaped, micro-tensile samples 5 x 5  $\mu\text{m}$  in cross sectional area and 17  $\mu\text{m}$  in length from the unirradiated and irradiated samples. All micro-tensile samples were tested at a quasi-static strain rate and the stress-strain curves were analysed to determine the mechanical properties. A close correlation was found between micro-tensile results and the bulk mechanical properties reported in the literature. Comparison between the unirradiated micro-tensile properties of W-5Re and W-5Ta with W showed that, as expected, W-5Re was softer than W whilst W-5Ta had only minor differences in micro-tensile properties compared with W. The micro-tensile results of the irradiated W, W-5Ta and W-5Re showed an increase in strength and an almost complete loss of ductility compared to the unirradiated samples. In comparing micro-tensile results to nanoindentation measurements, it was found that micro-tensile offers comparable level of precision in measurement of irradiation hardening among W, W-5Ta and W-5Re. The

implications of the results with respect to the future performance of tungsten-based materials in the divertors in fusion reactors are discussed in detail.

Keywords: tungsten-rhenium, tantalum, fusion, radiation, damage, Micro-tensile

# 1. Introduction

Tungsten is the leading candidate material for the divertor component of future DEMONstration fusion reactors [1] and is also the material of choice for the International Thermonuclear Experimental Reactor (ITER) [2] currently being constructed in Provence, France. The divertor components play a critical role of ensuring the continuous operation of a fusion reactor by filtering out helium “ash” from the deuterium-tritium fusion reaction. The divertor is made from a ring of “cassettes” located at the bottom of the tokamak. Tungsten plates strategically oriented on each divertor cassette face the hot plasma, cooling and filtering out helium ash accumulated on the periphery of the toroidal deuterium-tritium plasma [3]. The divertor is expected to experience the most extreme environment in a fusion reactor, withstanding operating temperatures of 1000 °C (in the event of accidents: 3000°C), neutron damage (4.4dpa/annum for DEMO), thermal neutron transmutation of tungsten (3.8 at.% rhenium, 1.38 at.% osmium and 0.9 at.% tantalum after 5 years in a power plant reactor) and damage from alpha particle bombardment [2,4–6]. Compared to other candidate materials for the divertor such as carbon (early model of JET in Culham), tungsten has many advantageous qualities, especially its high melting point and good thermal conductivity, relatively lower sputter, transmutation and activation rates, and low tritium retention [4,7,8]. Despite this, the already poor mechanical properties of tungsten can degrade further during operation from being exposed to radiation under high temperature [9]. The rates of degradation of tungsten’s various mechanical properties are not known and the mechanisms involved are the subject of extensive research by experimentalists and modellers.

Due to the complexity involved with studying neutron and helium ion effects simultaneously materials scientists have undertaken research on either neutron or helium ion effects to date. Thus far, neutron irradiation studies undertaken on tungsten using nuclear research reactors have identified the formation of *non-equilibrium* precipitates between tungsten and its major neutron transmutation by-product: rhenium (Re) [10–16]. For a tungsten 5 at.% Re alloy, sigma phase forms after ~1-2dpa neutron irradiation at 500 – 800°C, in conflict with the W-Re thermodynamic phase diagram which

anticipates a complete solid solution [17]. Such precipitates are exclusively irradiation induced and their presence has been found to significantly increase the hardness of the tungsten by  $\sim 4$  GPa [11,18]. Further studies on the irradiation of W-Re alloys have been undertaken via self-ion irradiation using tungsten ions as an analogue for neutron displacement damage [19–24]. These studies have identified semi-coherent Re metastable clusters post ion irradiation. Such clusters are softer and have a weaker hardening effect relative to sigma precipitates. The same studies also identified irradiation flux (dpa rate) as being crucial in formation of precipitates in W-Re alloy. Neutron damage to a level of 1dpa over the course of a year induced precipitate formation in W-5Re while 10dpa tungsten ion damage over 3 days could induce only Re clusters in the W-5Re alloy.

On the other hand, studies of helium ion irradiation of tungsten have been relatively less expansive than neutrons. Until the end of 2022, the vast majority of literature on helium irradiation of tungsten involves single energy helium ions with energies that penetrated into a depth of  $\sim 500$ nm [25–27]. These studies found the irradiation hardening to plateau at 5.5 GPa beyond  $10^{17}$  ions/cm<sup>2</sup> as the helium bubble density saturates with only its diameter increasing. In most studies of helium ion irradiation, nanoindentation is used to evaluate the mechanical properties which carries a certain degree of inaccuracy as the hardness data extracted from such a shallow depth is a mixture of the plastic response of both the irradiated layer and the unirradiated substrate. Moreover, whilst hardness measurement is an effective means of gauging radiation strengthening it does not provide direct insight into how yield stress, work hardening and elongation are affected by irradiation. This is so because it creates a 3-dimensional state of stress, as opposed to uniaxial stress in a pure tensile test. No studies have been undertaken whereby the investigators make use of alternative micro-mechanical testing methodologies such as micro-tensile testing to understand helium ion irradiation effects.

Due to the limitations of using nanoindentation alone to understand irradiation effects, in this study, we have applied both micro-tensile and nanoindentation testing to understand the mechanical response of tungsten before and after helium ion irradiation. Here, samples were irradiated using 6

MeV helium ions that had passed through an energy spreading system, designed to uniformly distribute radiation damage and helium atoms through a 10  $\mu\text{m}$  depth. Formation of a uniform helium damage layer over a greater depth in tungsten haven't been attempted before to the best of the authors' knowledge, which allows the authors to extract mechanical properties more accurately. Additionally, samples of W-5Re and W-5Ta alloys were irradiated in this study, in order to effectively simulate a later stage of neutron irradiation since Re and Ta are transmutation by-products of the neutron irradiation of tungsten. By studying these two alloys, we attempted to simulate helium migration, displacement damage and transmutation effects taking place within the divertor since there is very sparse literature to date comparing effect of Re and Ta on mechanical properties of W under helium ion irradiation. By performing micro-tensile and nanoindentation testing of helium ion irradiated pure tungsten, W-5Re and W-5Ta alloys, it was possible to determine the accuracy of micro-tensile testing results relative to bulk scale results and nanoindentation testing and quantify the effect of helium irradiation on the strength and ductility of tungsten-based materials.

## 2. Experimental

### 2.1 Materials and Sample Preparation

Pure tungsten, W-5wt.%Re and W-5wt.%Ta alloys were supplied from Plansee® as sheets 10 x 10mm in length and width and 1mm thick (except W-5at.%Re sheets which were 0.5mm thick). For ease of referencing, the pure tungsten, W-5wt.%Re and W-5wt.%Ta will be referred to as W, W-5Re and W-5Ta from this point onwards.

The plates were initially annealed in a vacuum tube furnace for 24 hours at 1,000°C and air cooled to room temperature to relieve internal stresses whilst avoiding recrystallisation. The expected mechanical properties of 1mm W sheet with 0.43  $\mu\text{m}$  diameter grain size (measured on cross-section

perpendicular to rolling direction) produced by sintering, hot rolling at temperatures above 1200°C and cold rolling at 1000°C are shown in Table 1 as reproduced from publications of Bonk and Reiser et al. [28,29]. Tensile data for W-5Re sheet were not available, but instead published results detailing tensile testing of Plansee® W-5Re 1.5 mm diameter wires are shown for grain size ~3 μm (when measured on cross section perpendicular to wire length) and annealed for 1 hour at 1000 °C[30]. Data could not be found in the literature for Plansee® W-5Ta as this is an experimental composition. However, studies by Nogami et al. [24] on W-5Ta from A.L.M.T. Corp produced by sintering and hot rolling followed by stress relief having grain size of 50 μm (measured on cross-section perpendicular to rolling direction) are reproduced in Table 1 as well.

	W (1mm thick. Plate) (Source: Plansee)	W-5Re (1.5mm diameter Wire) (Source: Plansee)	W-5Ta (4mm thick. Place) (Source: A.L.M.T. Corp)
Yield Strength (MPa)	1593	-	1120
Ultimate Tensile Strength (MPa)	1713	1375	1220
Elongation to UTS (mm/mm)	0.014	0.03	0.01
Elongation to Failure (mm/mm)	0.031	0.03	0.02

Table 1. Mechanical properties of W, W-5Re and W-5Ta metal sheets and wires as reported in the literature.

The plates of W, W-5Re and W-5Ta were ground using SiC grinding paper from 80 to 1,200 grit followed by a diamond cloth polish using 15, 3 and 1μm grit diamond paste. Finally, a ~100nm colloidal silica polish was applied to the plates to guarantee a finish suitable for electron microscopy analysis as well as ion irradiation. A Zeiss Ultraplus Scanning Electron Microscope (SEM) equipped with Oxford Instruments Nordly S EBSD detector was used to perform EBSD analysis on the as-polished W, W-5Re and W-5Ta samples. The EBSD pole figure maps for W, W-5Re and W-5Ta are displayed in Figure 1(a-c). The grain size measured from the SEM images for W, W-5Re and W-5Ta using the line intercept method were all in the range 1-3 μm. The Inverse Pole Figure (IPF) map for Euler angles and grain

orientation along the X, Y and Z directions are shown in Figure 1(a-c) for each material. It is apparent across all three materials that there is strong texturing present. IPF plots for the W-5Re sample show strong texture towards the {100} planes along the x, y and z axis. The IPF Z and IPF X plots for the W and W-5Ta samples, respectively, show about half of the grains are textured along the {100} plane with the other half being textured along the {111} plane. The rolling process applied to these samples in their production most likely introduced the textures observed here. Furthermore, Appendix 1(a,b), Appendix 2(a,b) and Appendix 3(a,b) present an enlarged Euler angle IPF maps along with the 3° and 10° angle grain boundaries for the Pure W, W-5Ta and W-5Re samples. The use of 3° was most appropriate to highlight sub-grains present in the micro-structure across the Pure W, W-5Ta and W-5Re samples since the material is highly textured already.

## 2.2 Irradiation Environment

The 2MV tandem STAR ion accelerator at the Australian Nuclear Science and Technology Organisation (ANSTO) was used to irradiate W, W-5Re and W-5Ta samples with 6MeV He<sup>2+</sup> to a fluence of  $5.6 \times 10^{17}$  ions/cm<sup>2</sup>. The irradiation took place at room temperature (25°C) and the energy of the He ions was attenuated via the use of Al foils, placed in between the path of the ion beam and the sample. This energy spreading system is made of a steel disk of 15 cm in diameter, and 1 mm thick, out of which 21 equal sectors were cut out, and each hollow sector was covered by an aluminium foil of particular thickness (except one sector left uncovered by the foil). The thickness of each Al foil was chosen to reduce the energy of the He ion by a specific quantity. Each foil thickness is either higher or lower than the adjacent foil by 0.8 or 1 µm. The simulation of radiation damage and helium concentration profile were calculated using the radiation damage simulation software: Stopping Range of Ions in Matter (SRIM) [31] using the Kinchin-Pease method using the mode: “ion distribution and quick calculation of damage”. The damage was estimated from the vacancies and the displacement energy used is 70eV

[32]. The results are displayed in Figure 2(a-b). At depths of 3 to 10  $\mu\text{m}$  below the W sample surface, SRIM predicts a plateau in displacement damage at  $\sim 0.6$  dpa and He concentration at  $\sim 11,000$  appm.

### 2.3 Micro-Tensile Testing

Dog-bone samples  $5 \times 5 \mu\text{m}^2$  in cross-sectional area,  $17 \mu\text{m}$  in length and having  $3 \mu\text{m}$  radius fillets at the corners (to minimize stress concentration) were milled using a Zeiss Auriga 60 Focused Ion Beam Scanning Electron Microscope (FIB-SEM). In fabricating a dog-bone tensile sample, a large  $\text{Ga}^+$  ion current of 20nA at 30kV was initially used to perform rough milling followed by smaller currents of 4nA at 30kV and 1nA at 30kV to achieve the final dog-bone dimensions. All unirradiated and irradiated micro-tensile samples were fabricated along the rolling direction of the material.

There is a total of 6 combinations of different material compositions (W, W5Re, W5Ta) and conditions (unirradiated, irradiated). For each combination, 3 dog-bone micro-tensile samples were fashioned totalling 18 micro-tensile samples in all. All samples were tested at low strain rates of  $1.5 \times 10^{-6} - 3.9 \times 10^{-6}$  /s in both the unirradiated and irradiated states. Each micro-tensile sample was analysed via EBSD before and after micro-tensile testing. The micro-tensile testing took place on a micro-test rig (MTR-3™) developed by MicroTesting Solutions® Ltd. (Hilliard, OH, USA). The micro-test rig was mounted within a Zeiss® Ultra Plus™ SEM which was used to image the micro-tensile samples at regular displacement intervals. For every micro-tensile test, the strain was derived from the SEM images via a MATLAB image correlation code which requires the user to specify identify the neck regions of the dog-bone and then calculates the changes in length between the two points across all images. The code is owned by MicroTesting Solutions so it cannot be shared in this manuscript. During testing of the sample, it was paused temporarily while the SEM image was being taken (requiring 20 seconds for a high-resolution image). The testing rig also output the displacement, time stamp and load as measured by the load-cell. The engineering stress experienced by the micro-tensile sample was calculated by dividing the load by the dog-bone cross-sectional area. The displacement was



calculated by the testing rig software using an equation that accounted for calibration parameters and the voltage experienced by the load cell. Previous, studies by Xu et al [33] found the displacement values to be linearly correlated with strain measurements from SEM.

## 2.4 Nanoindentation

An Agilent® G300 Nanoindenter fitted with a Berkovich diamond tip was used to probe the hardness of the W, W-5Ta and W-5Re samples before and after irradiation. The “hardness at depth” mode was applied and 1.2  $\mu\text{m}$  was the depth of choice for hardness measurement of all samples. The selection of 1.2  $\mu\text{m}$  makes it possible to overcome tip shape effects and indentation size effects present at depths below 0.2  $\mu\text{m}$  and is also a depth where the plastic zone (8-10  $\mu\text{m}$  radius as per findings of Saleh et al [34]) falls within the helium ion damage zone of 11  $\mu\text{m}$ , thus measuring the hardness response from exclusively the irradiation layer. For each sample 100 indents were performed and the mean and standard deviation calculated from the measurements.

## 3. Results

The engineering stress-strain plots from multiple micro-tensile samples of W, W-5Ta and W-5Re in the unirradiated and irradiated state are displayed in figure 3(a-c). The strain values were calculated from the SEM images of the dog-bone samples taken at regular intervals as detailed in §2.3.

Across all the engineering stress-strain plots presented, the unirradiated micro-tensile samples exhibited plasticity upon reaching the yield stress and necked upon reaching the ultimate tensile stress. However, there is no macro-plasticity present amongst the helium ion irradiated samples where the samples fracture at failure strains significantly lower than the unirradiated samples. Such

ductility present amongst the unirradiated W, W-5Ta and W-5Re is further emphasized in figure 4 (a), figure 5 (a) and figure 6 (a) where Inverse Pole Figure (IPF) plots of grain orientation relative to the tensile axis of micro-tensile samples before and after fracture are presented. In contrast, the embrittlement of W, W-5Ta and W-5Re after ion irradiation further evidenced in IPF plots in figure 4 (b), figure 5 (b) and figure 6 (b) respectively. All the micro-tensile samples presented in Figure 4 – 6 are oriented along the y-axis as labelled in Figure 1(a-c), the EBSD images of the bulk material.

The average values of the yield stress (YS) at 0.2% strain, ultimate tensile strength, strain to ultimate tensile strength (UTS) and strain to failure along with strain rate for all the stress-strain plots of W, W-5Re and W-5Ta samples presented in Figure 3(a-c) are summarised in table 2. All the values reported in table 2 are the engineering stress and strain values and the error values reported are calculated from the standard deviation of the data sets. Since the irradiated W, W-5Ta and W-5Re samples possessed no measurable ductility, there is no YS to report. Only the failure stress is reported as the UTS instead in table 2.

	YS (MPa)	UTS (MPa)	Failure Stress (MPa)	$\epsilon$ @ UTS	$\epsilon$ @ Fail	$\epsilon'$ ( $\times 10^{-6}/s$ )
W_UNIR	1403 $\pm$ 256	1581 $\pm$ 113	–	0.013 $\pm$ 0.003	0.273 $\pm$ 0.059	3.4 $\pm$ 0.5
W_HEIR	–	–	3423 $\pm$ 312	–	0.01 $\pm$ 0.004	1.5 $\pm$ 0.7
W5Ta_UNIR	1357 $\pm$ 164	1484 $\pm$ 117	–	0.013 $\pm$ 0.006	0.013 $\pm$ 0.006	3.9 $\pm$ 0.2
W5Ta_HEIR	–	–	2834 $\pm$ 145	–	0.009 $\pm$ 0.002	1.8 $\pm$ 0.3
W5Re_UNIR	1146 $\pm$ 39	1299 $\pm$ 37	–	0.032 $\pm$ 0.017	0.398 $\pm$ 0.032	2.1 $\pm$ 1.1
W5Re_HEIR	–	–	2488 $\pm$ 304	–	0.013 $\pm$ 0.003	1.8 $\pm$ 0.4

Table 2. Mechanical properties: yield stress (YS), ultimate tensile strength (UTS), strain to UTS and strain to failure and strain rate of micro-tensile samples of W, W-5Ta and W-5Re in unirradiated and irradiated condition (UNIR and HEIR respectively).

Nanoindentation measurements of the hardness of the W, W-5Ta and W5Re samples at 1.2  $\mu$ m depth are reported in Table 3 along with the error values (standard deviation). The irradiation hardening for each sample is also presented in Table 3 and is calculated by subtracting the unirradiated hardness from the irradiated hardness measurement. Also present in the table is the estimated increase in UTS from irradiation for each sample which is calculated by dividing the

irradiation hardening values by 3 (estimated Tabor factor). The increase in UTS from irradiation as calculated from micro-tensile (table 2) and nanoindentation (table 3) are visually represented in Figure 7 bar chart for W, W-5Ta and W-5Re

	Unirradiated Hardness (GPa)	Irradiated Hardness (GPa)	Irradiation Hardening (GPa)	Increase in UTS from Irradiation (GPa)
W	6.27 ± 0.33	8.87 ± 0.33	2.6 ± 0.46	0.87 ± 0.15
W5Ta	5.64 ± 0.44	7.55 ± 0.58	1.92 ± 0.73	0.64 ± 0.24
W5Re	5.22 ± 1.21	9.16 ± 0.32	3.94 ± 1.25	1.31 ± 0.42

Table 3. Nanoindentation hardness measurement of W, W-5Ta and W-5Re in unirradiated and irradiated state. Also presented here is the irradiation hardening and strengthening for each sample.

## 4. Discussion

### 4.1 Micro-tensile results vs bulk tensile properties

Micro-tensile testing of W and W-5Re (table 2) yielded results similar to those from the bulk materials as reported by the Plansee supplier in table 1. The W micro-tensile samples have a YS and UTS of  $1403 \pm 256$  and  $1580.77 \pm 113.33$  MPa respectively (table 2) which approaches the YS and UTS of bulk W plate (Table 1): 1593 and 1713 MPa respectively. Similarly, the W-5Re micro tensile samples measured a UTS of  $1299.45 \pm 36.67$  MPa, which matches the UTS reported for bulk W-5Re 1.5 mm diameter wires of 1375 MPa. The close correlation in strength between the micro-tensile samples and the bulk properties for W and W-5Re confirms the reliability of micro-tensile testing in reproducing bulk properties.

The replication of yield strength and UTS of tungsten on the micron scale extends to other mechanical properties, such as elongation. Table 2 reports the *strain at UTS* of the micro-tensile samples of unirradiated W and W-5Re which are  $0.013 \pm 0.003$  and  $0.032 \pm 0.017$  respectively. The values approach the elongation to UTS for bulk samples of W and W-5Re at 0.014 and 0.03 respectively (table 1). However, the W and W-5Re micro-tensile samples *failed* at  $0.273 \pm 0.059$  and  $0.398 \pm 0.032$  (table

2) respectively which did not reproduce bulk values (table 1). It is likely that shear strain is less constrained for the micro-tensile samples than for the bulk tensile samples reported in the literature, allowing for a greater degree of elongation to failure.

Meanwhile, there is discrepancy when in comparing the micro-tensile results for W-5Ta (Table 2) compared to the bulk tensile results for W-5Ta from Nogami et al. [24] in Table 1. The micro-tensile YS and UTS for W-5Ta are  $1357 \pm 164$  and  $1484 \pm 117$  MPa respectively which are larger than the bulk YS and UTS values in Table 1: 1120 and 1220 MPa. The difference can be largely attributed to the grain size of the bulk W-5Ta tested by Nogami et al, which is  $50 \mu\text{m}$  an order of magnitude greater than the grain size reported here. Thus, the Hall-Petch effect is likely the major reason for the difference in stress measured here and it is further evidenced in the YS and UTS reported for Pure Tungsten (grain size  $120 \mu\text{m}$ ) having a 880 MPa significantly lower than that measured for Pure Tungsten (grain size  $0.43 \mu\text{m}$ ) by Reiser et al. [29]. There is similarity in the elongation to UTS for W-5Ta but the difference grain size between the sample studied here from Plansee and Nogami's sample from A.L.M.T. corp make it difficult to compare between the two.

Overall, micro-tensile testing of W and W-5Re gave mechanical property values of yield strength, UTS and strain to UTS that replicated bulk mechanical properties reported in the literature. Such comparison highlights the usefulness of micro-tensile testing in ascertaining bulk properties and shows size-effects are absent at the micron level where there are more than 25 grains within the cross-sectional area. This is consistent with prior studies on Ni-3wt%SiC [35]. It is also supported by studies of Vo et al. [36] where micro-tensile testing of unirradiated and proton irradiated 304 stainless steel produced yield stress values that closely matched yield stress estimated from the nanoindentation hardness measurements. We therefore expect that the mechanical properties reported here for the irradiated W, W-5Ta and W-5Re will also be representative of bulk mechanical properties.

## 4.2 Comparison of mechanical properties of W, W-5Re and W-5Ta alloys.

In the unirradiated state, the presence of rhenium or tantalum in solid solution appears to have differing effects on tungsten. In figure 3(a-c) and table 2, the elongation to UTS for W-5Re is 3 times greater than that of W while the elongation to UTS for W-5Ta is the same as W. The W-5Re alloy has a lower UTS than W whilst W-5Ta has a similar UTS to W. In all, when comparing mechanical response of W-5Re to W, the presence of Re appears to increase the elongation to failure which is consistent with literature findings on Re addition to tungsten [37]. On the other hand, the W-5Ta alloy possesses mechanical properties similar to those of W which implies the presence of Ta to have a negligible effect on W mechanical properties at room temperature. There is a difference in texture between the pure W, W-5Re and W-5Ta samples but the inherent effect of Re and Ta solute elements appear to overcome this as we observed trends in mechanical properties that mirror the literature. Nonetheless, only qualitative comparison is possible at this point as the differences in texture do not allow for a detailed quantitative comparison of the effect of Re and Ta solute elements.

## 4.3 Effect of irradiation on W, W-5Re and W-5Ta alloys.

In this study, helium irradiation of W, W-5Re and W-5Ta to a radiation damage level of 0.6 dpa and helium concentration of 11,000 appm (figure 2) brought about embrittlement of the samples which is evidenced by the increase in failure stress and decrease in ductility. In figure 3(a-c) and table 2, there is a minimum two-fold increase in failure stress across all samples. This increase in strength between the irradiated and unirradiated state is particularly pronounced for W at  $1,842 \pm 332$  MPa as it is statistically greater than the strengthening observed for W-5Ta and W-5Re at  $1,350 \pm 186$  and  $1,188 \pm 307$  MPa respectively. The error bars overlap for the irradiation strengthening of W-5Ta and W-5Re samples, so it appears Ta and Re have similar irradiation response under the helium irradiation conditions used here.

The presence of Re or Ta reduces the degree of hardening from irradiation but, it has negligible impact on the reduction in ductility brought about by helium irradiation. Across W, W-5Re and W-5Ta, ductility almost completely disappeared post irradiation and all samples failed in a brittle manner. This contrast in ductility before and after irradiation is evident in EBSD images in figure 4(a-b), figure 5(a-b) and figure 6(a-b). The fractured micro-tensile sample for unirradiated W, W-5Re and W-5Ta all show a strong degree of grain rotation along with slip line formation occurring near the fractured surface, which indicates that ductile failure occurred. On the other hand, the fractured micro-tensile samples for irradiated W, W-5Re and W-5Ta feature no grain rotation or slip line formation. The micro-tensile samples all cleaved trans-granularly across the sample. The irradiated samples also exhibited small failure strains (table 2), an order of magnitude smaller than the failure strains recorded for the unirradiated samples.

The results presented here are significant as they bring to light three major findings that clarify previous helium ion irradiation studies of tungsten in the literature, which were based mainly upon hardness measurements. The first is that the presence of Re or Ta additions have a negligible effect on the embrittlement rate of tungsten. This is evidenced by the almost complete loss in ductility across all W, W-5Re and W-5Ta samples. This result dispels any notion that the inherent softening and ductilising effect Re have on W would be carried over under irradiation conditions. Secondly, whilst grain boundaries act as sinks for helium, they are not substantially weakened as a result of the helium accumulation and so do not become points of failure at this level of helium. This is demonstrated in the EBSD analysis of all the helium ion irradiated W, W-5Re and W-5Ta samples which consistently show trans-granular cleavage. Finally, irradiation hardening measured in tungsten from helium ion irradiation does equate to embrittlement. This is in good agreement with a similar study by Zhao et al [25], in which a tungsten plate was implanted with helium ions to a fluence similar in order of magnitude ( $3 \times 10^{17}$  ions/cm<sup>2</sup>) to the fluence used here. Zhao et al measured the ratio in hardness of the irradiated to unirradiated tungsten to be  $\sim 2$ , very similar to the value determined here for micro-tensile specimens: 2.2. As such, the elongation to failure afforded by micro-tensile testing shows the

irradiation hardening brought about by helium bubble formation results in severe embrittlement of the materials. All findings reported here are restricted to room temperature helium ion implantation and testing, the micro-tensile performance of these alloys at higher temperatures is unknown and yet to be investigated.

The findings reported here raise a point of concern for tungsten divertors within fusion reactors. During the operation of the proposed DEMO fusion reactor, the helium plasma that bombards the tungsten divertor armour is expected to vary in energy from tens to millions of eV with a large flux of  $10^{18} - 10^{20}$  ions/cm<sup>2</sup>/s [38]. Under such conditions, the fluence used in this study of  $5.6 \times 10^{17}$  ions/cm<sup>2</sup> would be achieved within merely half a second. Within such a small time-frame and even at room temperature, the tungsten in the sub-micron region immediately below the surface of the divertor armour would quickly become embrittled as a result of helium implantation. At operating temperatures of 1000°C where vacancies are mobile [39] and assist in formation of bubbles at grain boundaries [40,41], it is likely tungsten will fail intergranularly and embrittle to a greater extent. The micro-tensile performance of Pure W, W-5Ta and W-5Re under helium ion implantation at temperatures above the vacancy activation temperature is subject of investigation by the authors. The study presented here where only self-interstitials and helium migration dominate serves as a reference point in appreciating the role of vacancies when they are mobile at temperatures above 470°C [21,39,42].

#### 4.4 Comparison of micro-tensile and nanoindentation results

Micro-tensile testing was able to determine differences in mechanical properties between W and W-5Re and W-5Ta compared to nanoindentation. As figure 7 shows, the irradiation strengthening measured for micro-tensile tests featured a spread of results similar in magnitude to the corresponding spread for nanoindentation tests even though the sample size for micro-tensile is 3 – 5 compared to 75 – 100 for the indents. Thus, micro-tensile testing can achieve at least the same degree

of precision in measurement of UTS compared to nanoindentation. Interestingly, micro-tensile testing can reveal at a statistically significant level the lower degree of increase in UTS where Re or Ta is present, compared to pure W. In comparing the irradiation hardening values reported between micro-tensile and nanoindentation for W and W-5Ta, the nanoindentation reports a hardening value that is nearly half that of the micro-tensile results. It is suspected that there is an asymmetrical mechanical response in compression stress state of nanoindentation compared to the tensile stress state of micro-tensile testing. The authors have observed this behaviour in other materials when comparing nanoindentation and micro-tensile testing and is a subject of investigation. Moreover, this anomaly relating to nanoindentation and micro-tensile testing have been previously observed in a study by Yu et al. [43] where tungsten was irradiated to 1dpa with self-ions at 500 and 800 °C after which Yu et al. measured the strength and hardness by micro-tensile and nanoindentation respectively. In their publication, the hardness values at 1dpa 500 °C and 800 °C closely approach each other, implying that the irradiation temperature has little effect on irradiation hardening. This was in contrast to the UTS values measured via micro-tensile testing where the 1dpa 800C sample showed greater degree of hardening than the 1dpa 500 °C samples. Clearly, micro-tensile testing can complement nanoindentation very well to reveal otherwise hidden trends.

## 5. Conclusions

In this study, the authors successfully used micro-tensile testing to investigate the mechanical properties of W, W-5Ta and W-5Re in the unirradiated state and room temperature helium ion irradiated state. The results are compared to those obtained from nanoindentation tests. Key findings are as follows:

- Micro-tensile testing is capable of reproducing bulk mechanical properties of tungsten and its alloys provided the cross-section of the sample contains at least ~25 grains. The yield stress and elongation to failure as measured for micro-tensile samples of W and W-5Re closely



mirrored the bulk properties reported in the literature. The success of this work justifies the use of micro-tensile testing in future ion irradiation tests for understanding performance of tungsten under fusion reactor environments.

- The presence of Re in W produces, as expected, a strong softening and ductilising effect. This is evidenced by lower yield stress and higher elongation to failure in W-5Re compared to W. On the other hand, Ta has negligible effect on the mechanical properties of W, only the strain hardening coefficient appears to have increased relative to W-5Re at a statistically significant level.
- Helium irradiation of W, W-5Re and W-5Ta at room temperature brings about an increase by a factor of two in strength, and severe embrittlement of the alloys. Unirradiated samples failed in a ductile manner demonstrated by the grain rotation and slip line formation shown in SEM and EBSD analysis. Post irradiation, all micro-tensile samples failed in a brittle manner within the elastic regime. SEM and EBSD analysis showed an absence of slip lines or grain rotation. This study confirms that irradiation hardening measured in W and its alloys, as reported in the literature, coincides with embrittlement of W.
- The presence of Re and Ta which are expected transmutation by-products of W operating under fusion conditions, reduce the extent of increase in strength after helium ion irradiation at room temperature. However, Re and Ta presence does not provide any radiation damage resistance because W-5Re and W-5Ta both exhibit the same degree of ductility loss as W.
- Despite the helium accumulation anticipated along grain boundaries as reported in the literature in helium ion implanted tungsten, tungsten grain boundaries do not act as points of weakness. This is evidenced in the transgranular failure observed in both unirradiated and helium irradiated (room temperature) micro-tensile samples of W, W-5Re and W-5Ta.
- Micro-tensile testing offers same level of precision in measurement of YS and UTS compared to nanoindentation. There is a discrepancy in measurement of irradiation hardening for micro-

tensile testing vs nanoindentation which have been observed in previous studies. This is a subject of ongoing research.

## Acknowledgements

The authors would like to express their sincere gratitude to Nuclear Fuel Cycle (NFC), Nuclear Materials Development and Characterization group (NMDC) and Colin Hobman from the Maintenance Workshop at ANSTO for their advice and help on sample preparation related issues. Sincere thanks are also due to Dr. Robert Wheeler of MicroTesting Solutions LLC<sup>®</sup>, OH, for many fruitful discussions and suggestions.

## Author Contributions

AX designed the experiments and performed the annealing, micro-mechanical testing, nanoindentation and EBSD analysis and subsequent data analysis. AX also drafted the original paper. TW and MI helped with ion irradiation and scientific discussions. TP grinded and polished the tungsten samples. KS assisted with nanoindentation. DA provided materials and scientific discussions. DB and GS reviewed and edited the original manuscript.

## Funding

This project was funded by internal research funding from the Nuclear Fuel Cycle.

## Data Availability

The raw/processed data required to reproduce these findings can be shared upon request.

## Supplementary Information

Additional EBSD images to support the observations made on Figure 1(a-c) is provided in Appendix 1-

3.

## Declarations

**Conflict of Interest:** The authors declare they have no competing research or financial interests that affects the quality of the work presented here.

**Ethical approval:** This paper does not involve experiments on humans or animals.

## References

- [1] D. Stork, P. Agostini, J.L. Boutard, D. Buckthorpe, E. Diegele, S.L. Dudarev, C. English, G. Federici, M.R. Gilbert, S. Gonzalez, A. Ibarra, C. Linsmeier, A. Li Puma, G. Marbach, P.F. Morris, L.W. Packer, B. Raj, M. Rieth, M.Q. Tran, D.J. Ward, S.J. Zinkle, Developing structural, high-heat flux and plasma facing materials for a near-term DEMO fusion power plant: The EU assessment, *J. Nucl. Mater.* 455 (2014) 277–291. doi:10.1016/j.jnucmat.2014.06.014.
- [2] J.W. Davis, V.R. Barabash, A. Makhankov, L. Ploch, K.T. Slattery, Assessment of tungsten for use in the ITER plasma facing components, *J. Nucl. Mater.* 258–263 (1998) 308–312.
- [3] S. Griffith, ITER divertor under final review (<http://www.iter.org>), 2012 (2012).
- [4] M.R. Gilbert, J.-C. Sublet, Neutron-induced transmutation effects in W and W-alloys in a fusion environment, *Nucl. Fusion.* 51 (2011) 13.
- [5] M.R. Gilbert, S.L. Dudarev, S. Zheng, L.W. Packer, J.-C. Sublet, An integrated model for materials in a fusion power plant: transmutation, gas production, and helium embrittlement under neutron irradiation, *Nuclear Fusion.* 52 (2012) 12.
- [6] C.S. Becquart, C. Domain, A density functional theory assessment of the clustering behaviour of He and H in tungsten, *J. Nucl. Mater.* 386–388 (2009) 109–111. doi:10.1016/j.jnucmat.2008.12.085.
- [7] S.W.H. Yih, C.T. Wang, *Tungsten: Sources, Metallurgy, Properties and Applications*, Plenum Press, New York, 1979.
- [8] G.D. Rieck, *Tungsten and its compounds*, Pergamon Press, Oxford, UK, 1967.
- [9] R.G. Abernethy, J.S.K.L. Gibson, A. Giannattasio, J.D. Murphy, O. Wouters, S. Bradnam, L.W. Packer, M.R. Gilbert, M. Klimenkov, M. Rieth, H.C. Schneider, C.D. Hardie, S.G. Roberts, D.E.J. Armstrong, Effects of neutron irradiation on the brittle to ductile transition in single crystal tungsten, *J. Nucl. Mater.* 527 (2019) 151799. doi:10.1016/j.jnucmat.2019.151799.

- [10] T. Tanno, A. Hasegawa, M. Fujiwara, J. He, S. Nogami, M. Satou, T. Shishido, K. Abe, Precipitation of solid transmutation elements in irradiated tungsten alloys, *Mater. Trans.* 49 (2008) 2259–2264.
- [11] T. Tanno, A. Hasegawa, J. He, M. Fujiwara, M. Satou, S. Nogami, K. Abe, T. Shishido, Effects of transmutation elements on the microstructural evolution and electrical resistivity of neutron-irradiated tungsten, *J. Nucl. Mater.* 386 (2009) 218–221.
- [12] Y. Nemoto, A. Hasegawa, M. Satou, K. Abe, Microstructural development of neutron irradiated W-Re alloys, *J. Nucl. Mater.* 283–287 (2000) 1144–1147.
- [13] A. Hasegawa, T. Tanno, S. Nogami, M. Satou, Property change mechanism in tungsten under neutron irradiation, *J. Nucl. Mater.* 417 (2011) 491–494.
- [14] E. Gaganidze, A. Chauhan, H.C. Schneider, D. Terentyev, B. Rossaert, J. Aktaa, Effect of irradiation temperature on the fracture-mechanical behaviour of tungsten irradiated to 1 dpa, *J. Nucl. Mater.* 556 (2021) 153200. doi:10.1016/J.JNUCMAT.2021.153200.
- [15] C. Yin, D. Terentyev, T. Zhang, S. Nogami, S. Antusch, C.C. Chang, R.H. Petrov, T. Pardoën, Ductile to brittle transition temperature of advanced tungsten alloys for nuclear fusion applications deduced by miniaturized three-point bending tests, *Int. J. Refract. Met. Hard Mater.* 95 (2021) 105464. doi:10.1016/J.IJRMHM.2020.105464.
- [16] S. Nogami, D. Terentyev, A. Zinovev, C. Yin, M. Rieth, G. Pintsuk, A. Hasegawa, Neutron irradiation tolerance of potassium-doped and rhenium-alloyed tungsten, *J. Nucl. Mater.* 553 (2021) 153009. doi:10.1016/J.JNUCMAT.2021.153009.
- [17] M. Ekman, K. Persson, G. Grimvall, phase diagram and lattice instability in tungsten-rhenium alloys, *J. Nucl. Mater.* 278 (2000) 273–276.
- [18] T. Tanno, A. Hasegawa, J. He, M. Fujiwara, S. Nogami, M. Satou, T. Shishido, K. Abe, Effects of transmutation elements on neutron irradiation hardening of tungsten, *Mater. Trans.* 48

- (2007) 2399–2402.
- [19] D.E.J. Armstrong, X. Yi, E.A. Marquis, S.G. Roberts, Hardening of self ion implanted tungsten and tungsten 5-wt% rhenium, *J. Nucl. Mater.* 432 (2013) 428–436.
- [20] A. Xu, D.E.J. Armstrong, C. Beck, M.P. Moody, G.D.W. Smith, P.A.J. Bagot, S.G. Roberts, Ion-irradiation induced clustering in W-Re-Ta, W-Re and W-Ta alloys: An atom probe tomography and nanoindentation study, *Acta Mater.* 124 (2017) 71–78.  
doi:10.1016/J.ACTAMAT.2016.10.050.
- [21] A. Xu, C. Beck, D.E.J. Armstrong, K. Rajan, G.D.W. Smith, P.A.J. Bagot, S.G. Roberts, Ion-irradiation-induced clustering in W-Re and W-Re-Os alloys: A comparative study using atom probe tomography and nanoindentation measurements, *Acta Mater.* 87 (2015) 121–127.  
doi:10.1016/j.actamat.2014.12.049.
- [22] R.W. Harrison, G. Greaves, J.A. Hinks, S.E. Donnelly, Intermetallic Re phases formed in ion irradiated WRe alloy, *J. Nucl. Mater.* 514 (2019) 123–127.  
doi:10.1016/J.JNUCMAT.2018.11.021.
- [23] T. Hwang, M. Fukuda, S. Nogami, A. Hasegawa, H. Usami, K. Yabuuchi, K. Ozawa, H. Tanigawa, Effect of self-ion irradiation on hardening and microstructure of tungsten, *Nucl. Mater. Energy.* 9 (2016) 430–435. doi:10.1016/J.NME.2016.06.005.
- [24] S. Nogami, I. Ozawa, D. Asami, N. Matsuta, S. Nakabayashi, S. Baumgärtner, P. Lied, K. Yabuuchi, T. Miyazawa, Y. Kikuchi, M. Wirtz, M. Rieth, A. Hasegawa, Tungsten–tantalum alloys for fusion reactor applications, *J. Nucl. Mater.* 566 (2022) 153740.  
doi:10.1016/J.JNUCMAT.2022.153740.
- [25] M. Zhao, F. Liu, Z. Yang, Q. Xu, F. Ding, X. Li, H. Zhou, G.N. Luo, Fluence dependence of helium ion irradiation effects on the microstructure and mechanical properties of tungsten, *Nucl. Instruments Methods Phys. Res. Sect. B Beam Interact. with Mater. Atoms.* 414 (2018) 121–

125. doi:10.1016/j.nimb.2017.09.002.
- [26] F. Kong, M. Qu, S. Yan, A. Zhang, S. Peng, J. Xue, Y. Wang, Helium-induced hardening effect in polycrystalline tungsten, *Nucl. Instruments Methods Phys. Res. Sect. B Beam Interact. with Mater. Atoms.* 406 (2017) 643–647. doi:10.1016/j.nimb.2017.02.029.
- [27] Z. Chen, L.L. Niu, Z. Wang, L. Tian, L. Kecskes, K. Zhu, Q. Wei, A comparative study on the in situ helium irradiation behavior of tungsten: Coarse grain vs. nanocrystalline grain, *Acta Mater.* 147 (2018) 100–112. doi:10.1016/j.actamat.2018.01.015.
- [28] S. Bonk, J. Hoffmann, A. Hoffmann, J. Reiser, Cold rolled tungsten (W) plates and foils: Evolution of the tensile properties and their indication towards deformation mechanisms, *Int. J. Refract. Met. Hard Mater.* 70 (2018) 124–133. doi:10.1016/j.ijrmhm.2017.09.007.
- [29] J. Reiser, J. Hoffmann, U. Jäntschi, M. Klimenkov, S. Bonk, C. Bonnekoh, A. Hoffmann, T. Mrotzek, M. Rieth, Ductilisation of tungsten (W): On the increase of strength AND room-temperature tensile ductility through cold-rolling, *Int. J. Refract. Met. Hard Mater.* 64 (2017) 261–278. doi:10.1016/J.IJRMHM.2016.10.018.
- [30] G. Kneringer, P. Rodhammer, H. Wildner, 15th International Plansee Seminar 2001 Vol1, 2001. [https://inis.iaea.org/collection/NCLCollectionStore/\\_Public/32/053/32053122.pdf](https://inis.iaea.org/collection/NCLCollectionStore/_Public/32/053/32053122.pdf) (accessed May 13, 2020).
- [31] J.F. Ziegler, M.D. Ziegler, J.P. Biersack, SRIM - The stopping and range of ions in matter (2010), *Nucl. Instruments Methods Phys. Res. B.* 268 (2010) 1818–1823.
- [32] A.Y. Konobeyev, U. Fischer, Y.A. Korovin, S.P. Simakov, Evaluation of effective threshold displacement energies and other data required for the calculation of advanced atomic displacement cross-sections, *Nucl. Energy Technol.* 3 (2017) 169–175. doi:<https://doi.org/10.1016/j.nucet.2017.08.007>.
- [33] A. Xu, M. Saleh, J. Davis, L. Edwards, D. Bhattacharyya, In-situ micro-tensile investigation of



- strain rate response along  $\langle 100 \rangle$  and  $\langle 110 \rangle$  directions in single crystal nickel, *Int. J. Plast.* 106 (2018) 129–144. doi:<https://doi.org/10.1016/j.ijplas.2018.03.005>.
- [34] M. Saleh, A. Xu, C. Hurt, M. Ionescu, J. Daniels, P. Munroe, L. Edwards, D. Bhattacharyya, Oblique cross-section nanoindentation for determining the hardness change in ion-irradiated steel, *Int. J. Plast.* 112 (2019). doi:10.1016/j.ijplas.2018.08.015.
- [35] A. Xu, C. Yang, G. Thorogood, D. Bhattacharyya, Investigating bulk mechanical properties on a micro-scale: Micro-tensile testing of ultrafine grained Ni–SiC composite to determine its fracture mechanism and strain rate sensitivity, *J. Alloys Compd.* 817 (2020). doi:10.1016/j.jallcom.2019.152774.
- [36] H.T. Vo, A. Reichardt, D. Frazer, N. Bailey, P. Chou, P. Hosemann, In situ micro-tensile testing on proton beam-irradiated stainless steel, *J. Nucl. Mater.* 493 (2017) 336–342. doi:<https://doi.org/10.1016/j.jnucmat.2017.06.026>.
- [37] P.L. Raffo, Yielding and fracture in tungsten and tungsten-rhenium alloys, (1968) 39. <https://ntrs.nasa.gov/api/citations/19680015005/downloads/19680015005.pdf>.
- [38] K. Wang, R.P. Doerner, M.J. Baldwin, C.M. Parish, Flux and fluence dependent helium plasma-materials interaction in hot-rolled and recrystallized tungsten, *J. Nucl. Mater.* 510 (2018) 80–92. doi:10.1016/J.JNUCMAT.2018.07.048.
- [39] D.N. Seidman, On the point-defect annealing mechanism for stage III recovery in irradiated or quenched tungsten, *Scr. Metall.* 13 (1979) 251–257.
- [40] W. Guo, L. Cheng, G. De Temmerman, Y. Yuan, G.H. Lu, Retarded recrystallization of helium-exposed tungsten, *Nucl. Fusion.* 58 (2018) 106011. doi:10.1088/1741-4326/AAD2B0.
- [41] M.A.T. Thompson, K. Song, G. De Temmerman, H. Chen, N. Kirby, J. Bradby, D. Bhattacharyya, C. Hoang, C.S. Corr, Identifying microstructural changes responsible for retarded grain growth during tungsten recrystallization after helium plasma exposure, *J. Nucl. Mater.* 559 (2022)

153448. doi:10.1016/J.JNUCMAT.2021.153448.

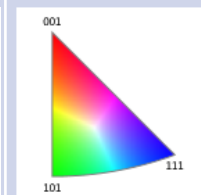
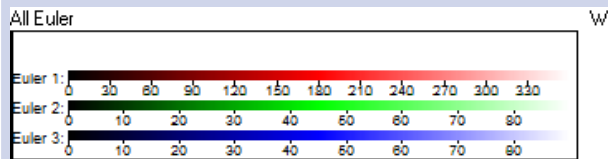
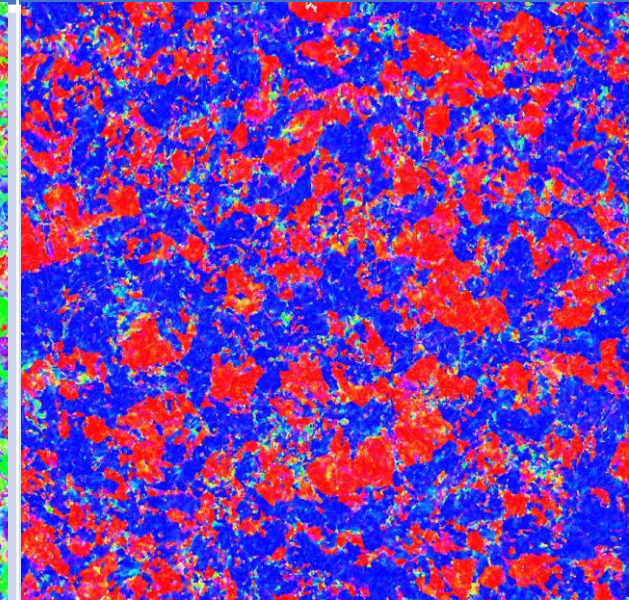
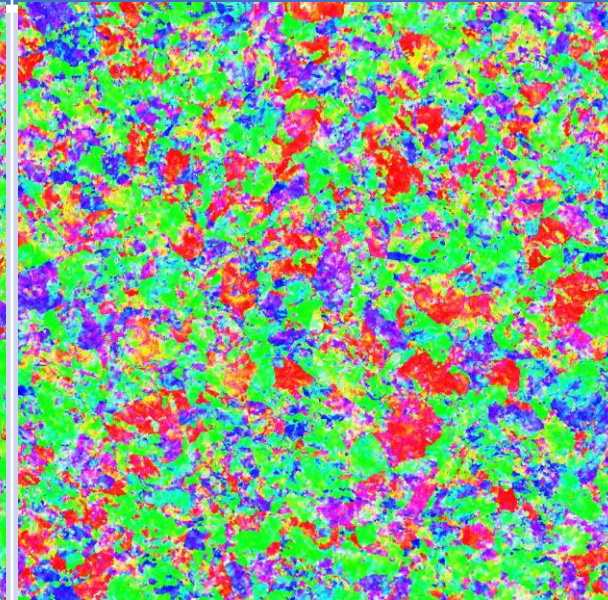
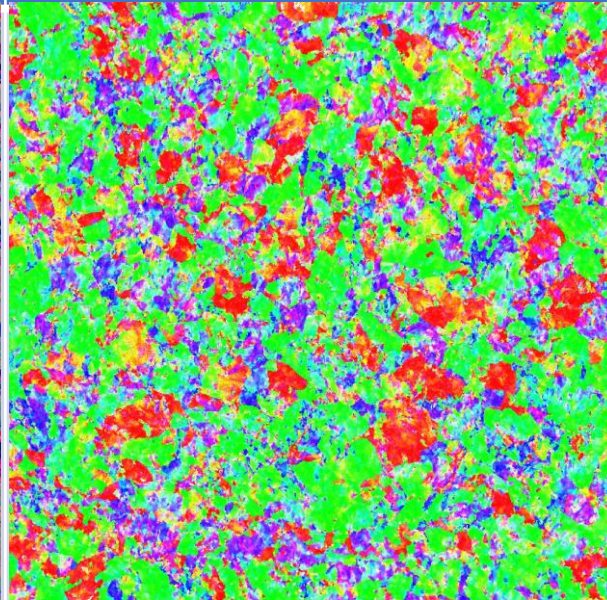
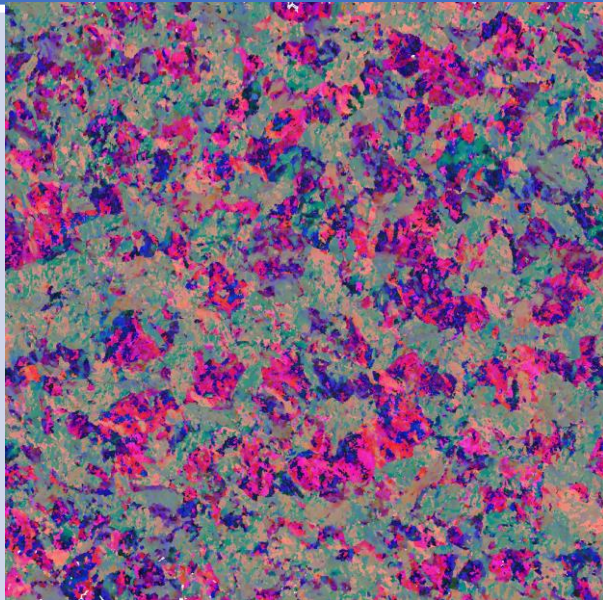
- [42] A. Xu, D.E.J. Armstrong, C. Beck, M.P. Moody, G.D.W. Smith, P.A.J. Bagot, S.G. Roberts, Ion-irradiation induced clustering in W-Re-Ta, W-Re and W-Ta alloys: An atom probe tomography and nanoindentation study, *Acta Mater.* 124 (2017). doi:10.1016/j.actamat.2016.10.050.
- [43] J.H. Yu, H. Kurotaki, M. Ando, T. Nozawa, Mechanical properties of self-ion irradiated pure tungsten using nano-indentation test and micro-tensile test, *Nucl. Mater. Energy.* 30 (2022) 101145. doi:10.1016/J.NME.2022.101145.

Euler

IPF X

IPF Y

IPF Z



250 $\mu$ m

Figure 1 (a). SEM images and EBSD pole figure of pure W along X, Y and Z direction.



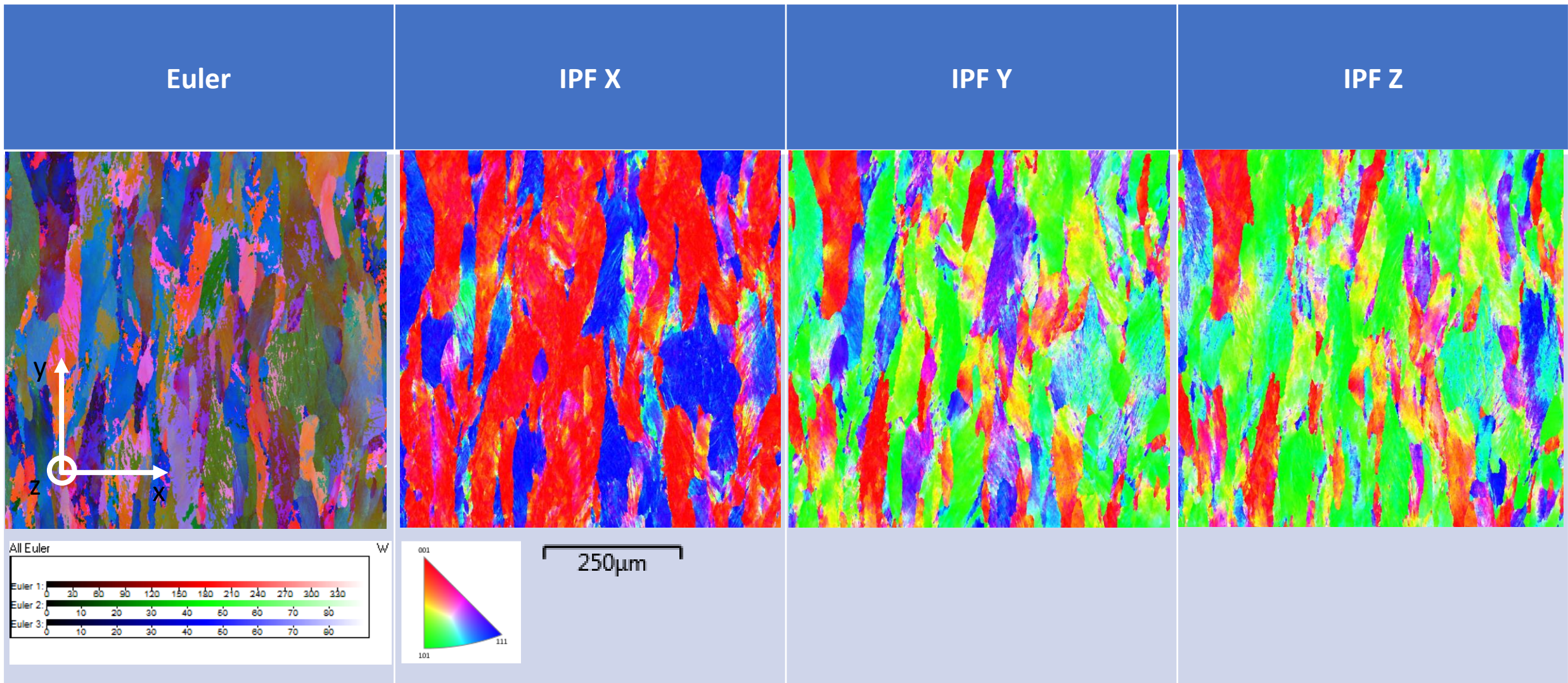


Figure 1 (b). SEM images and EBSD pole figure of W-5Ta along X, Y and Z direction.



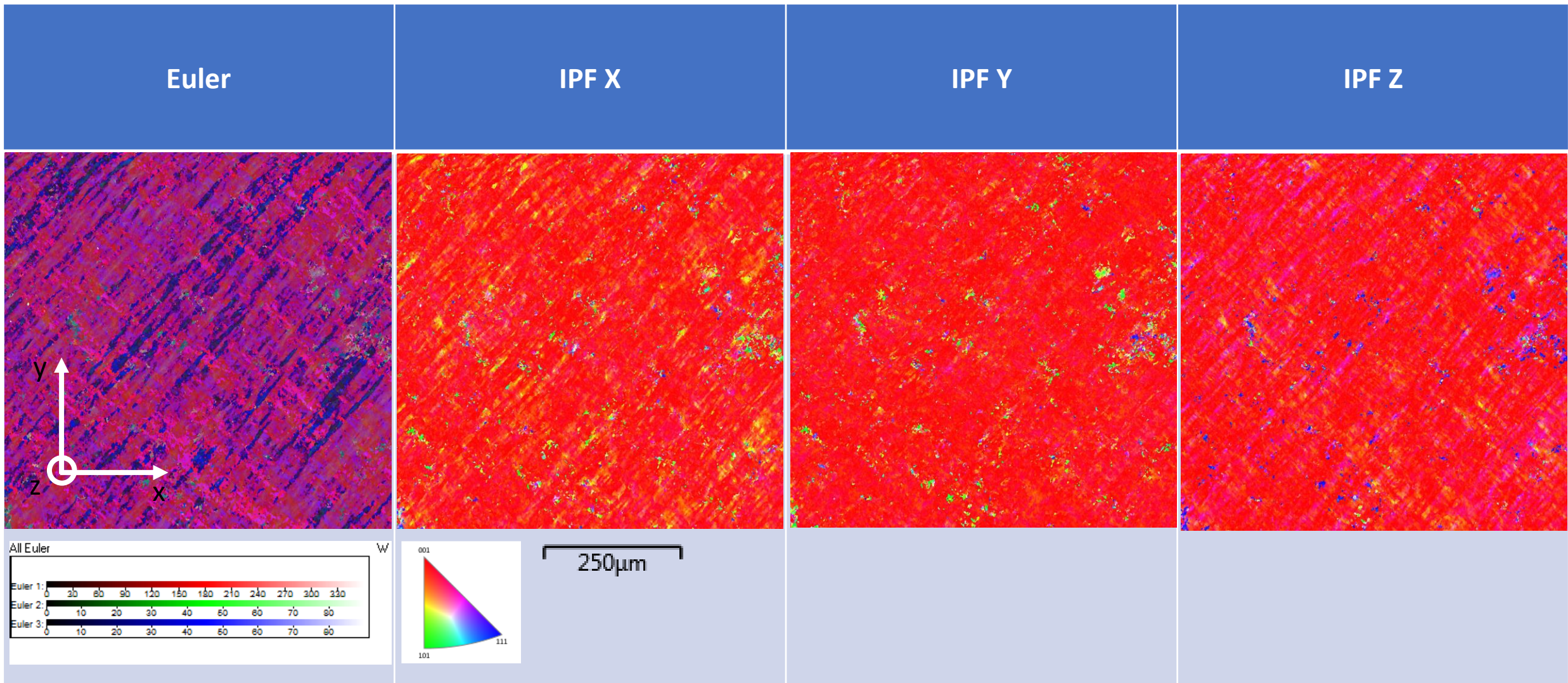


Figure 1 (c). SEM images and EBSD pole figure of W-5Re along X, Y and Z direction.

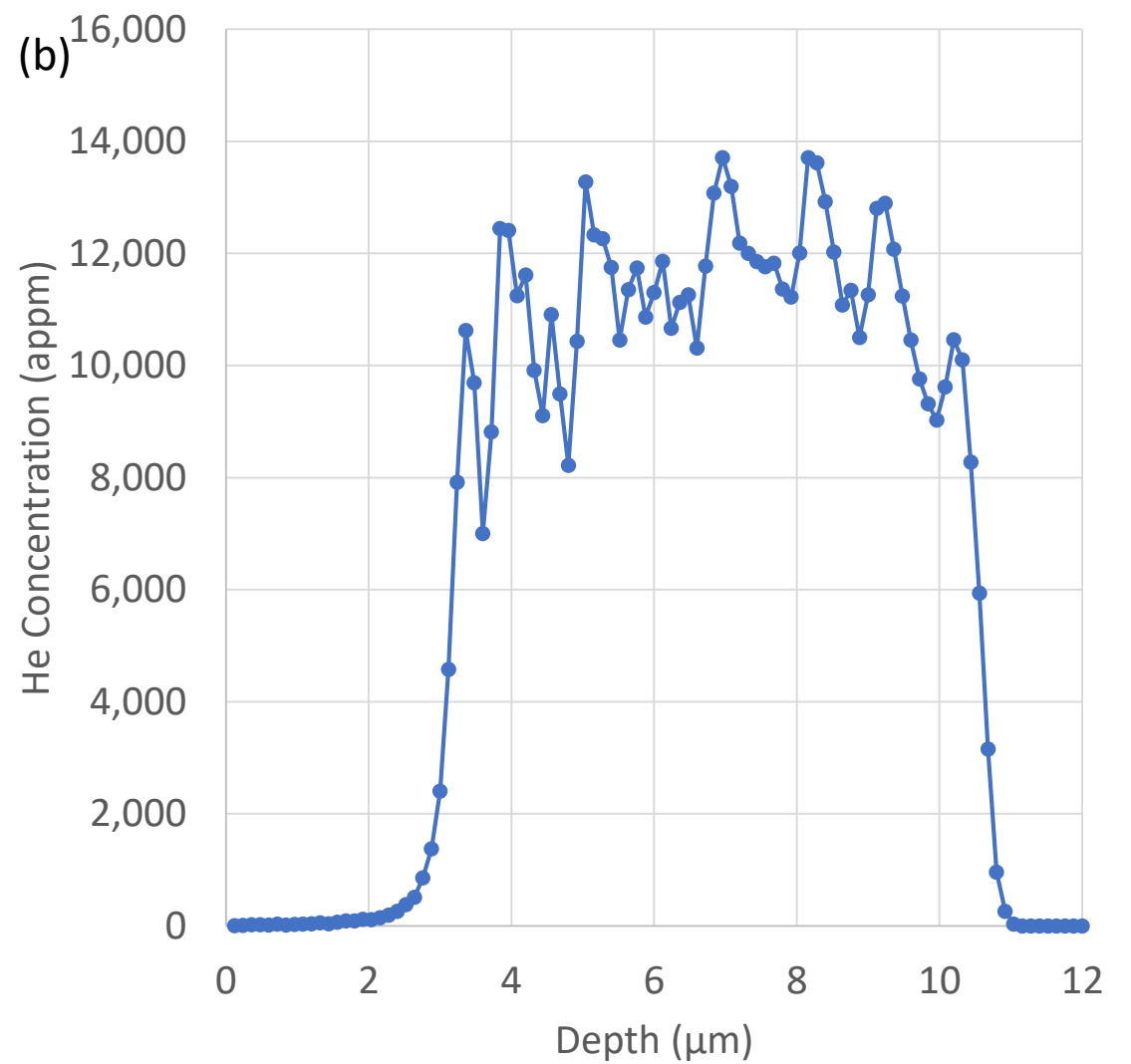
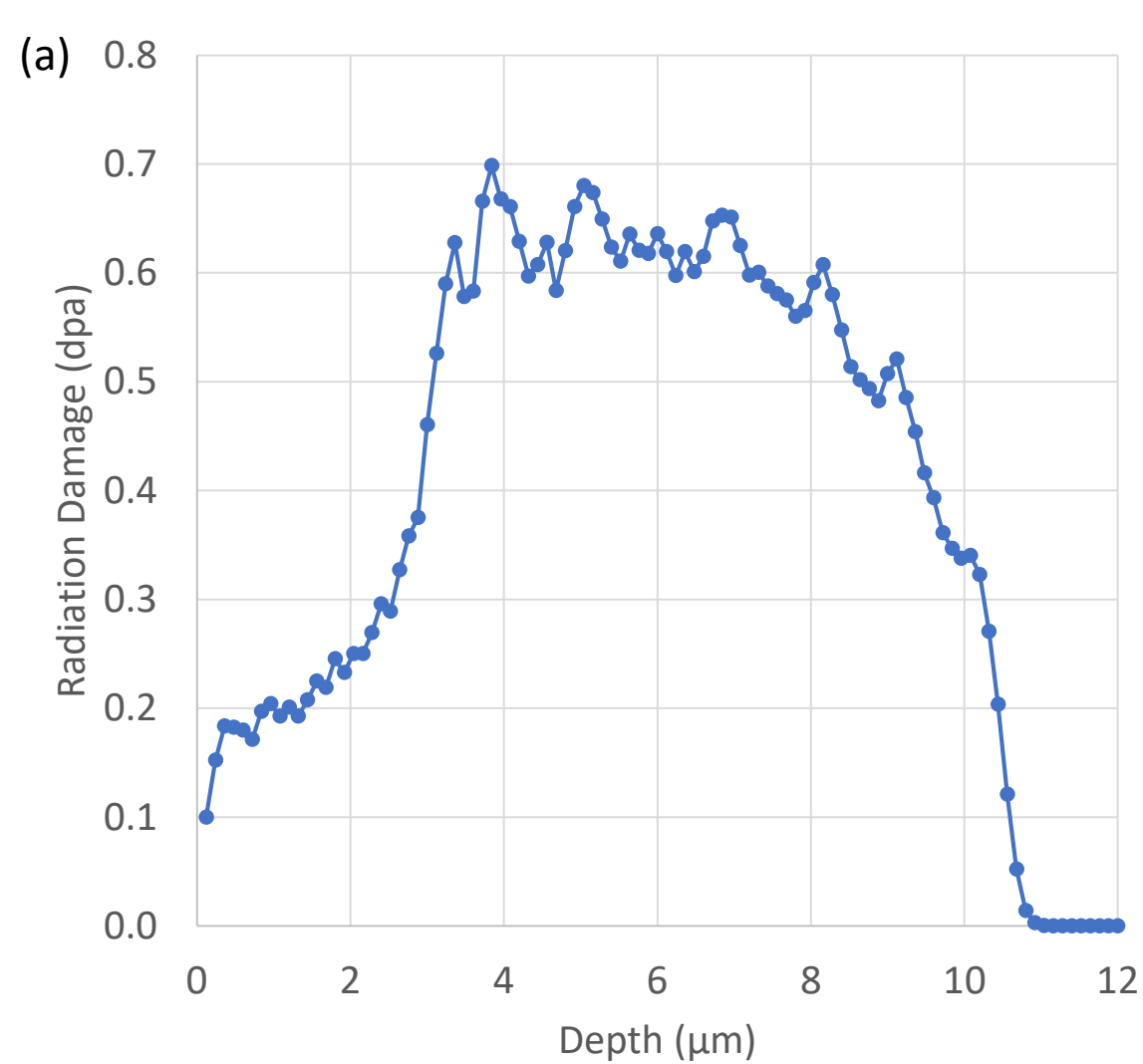


Figure 2. SRIM simulation of (a) radiation damage and (b) helium concentration depth profile of 6 MeV He ions implanted into pure W via an energy dispersion device.

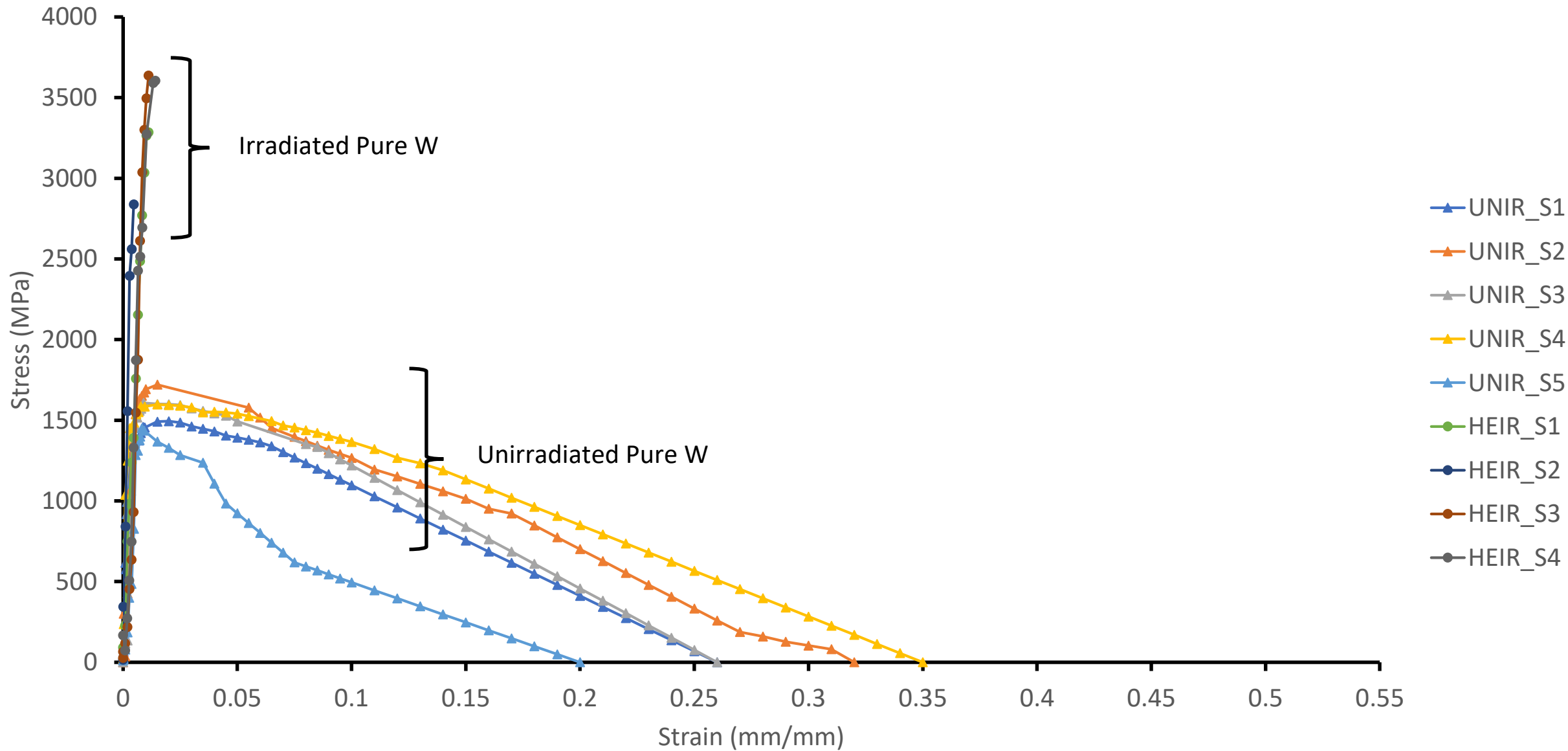


Figure 3 (a) Stress-strain plot of micro-tensile samples of Pure W for unirradiated (UNIR) and helium ion irradiated (HEIR).

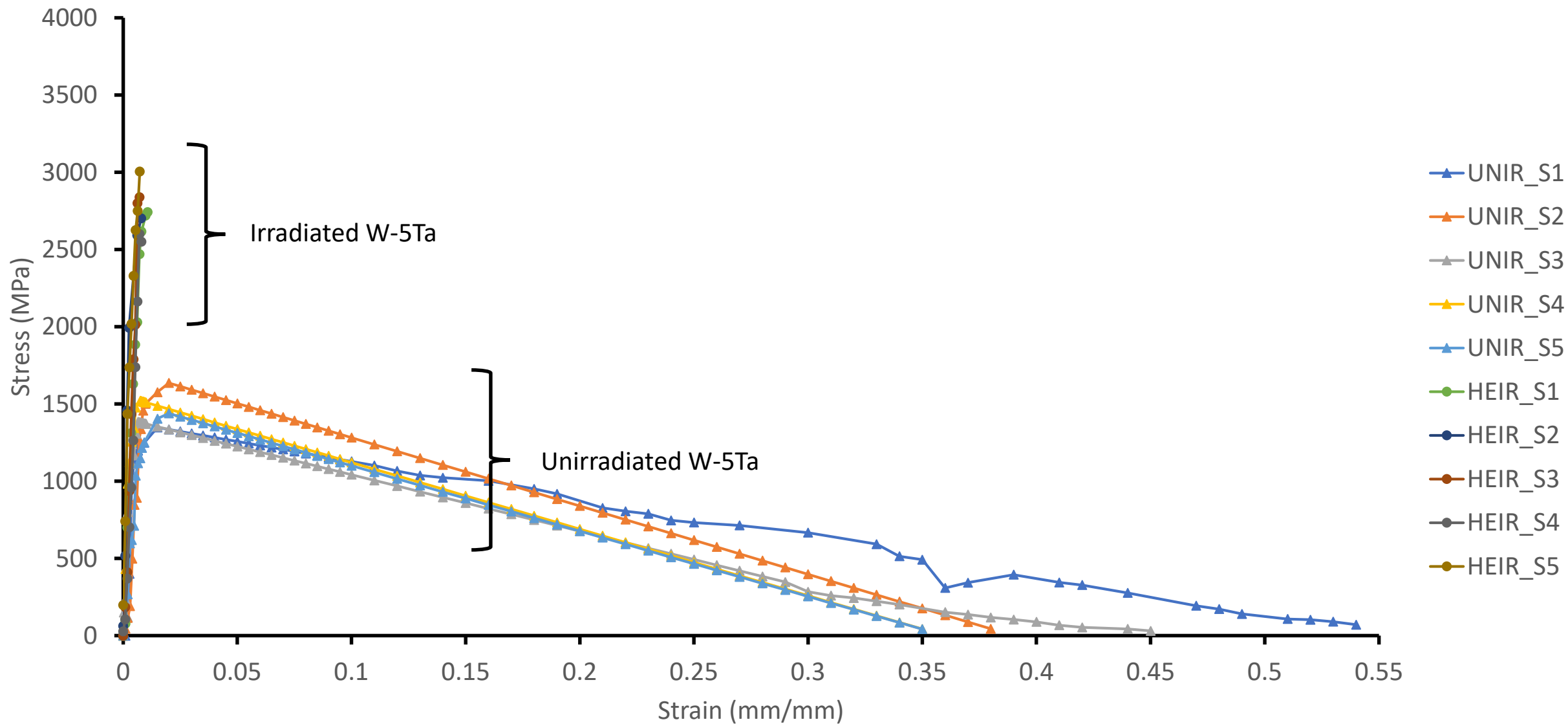


Figure 3 (b) Stress-strain plot of micro-tensile samples of W-5Ta alloys unirradiated (UNIR) and helium ion irradiated (HEIR).



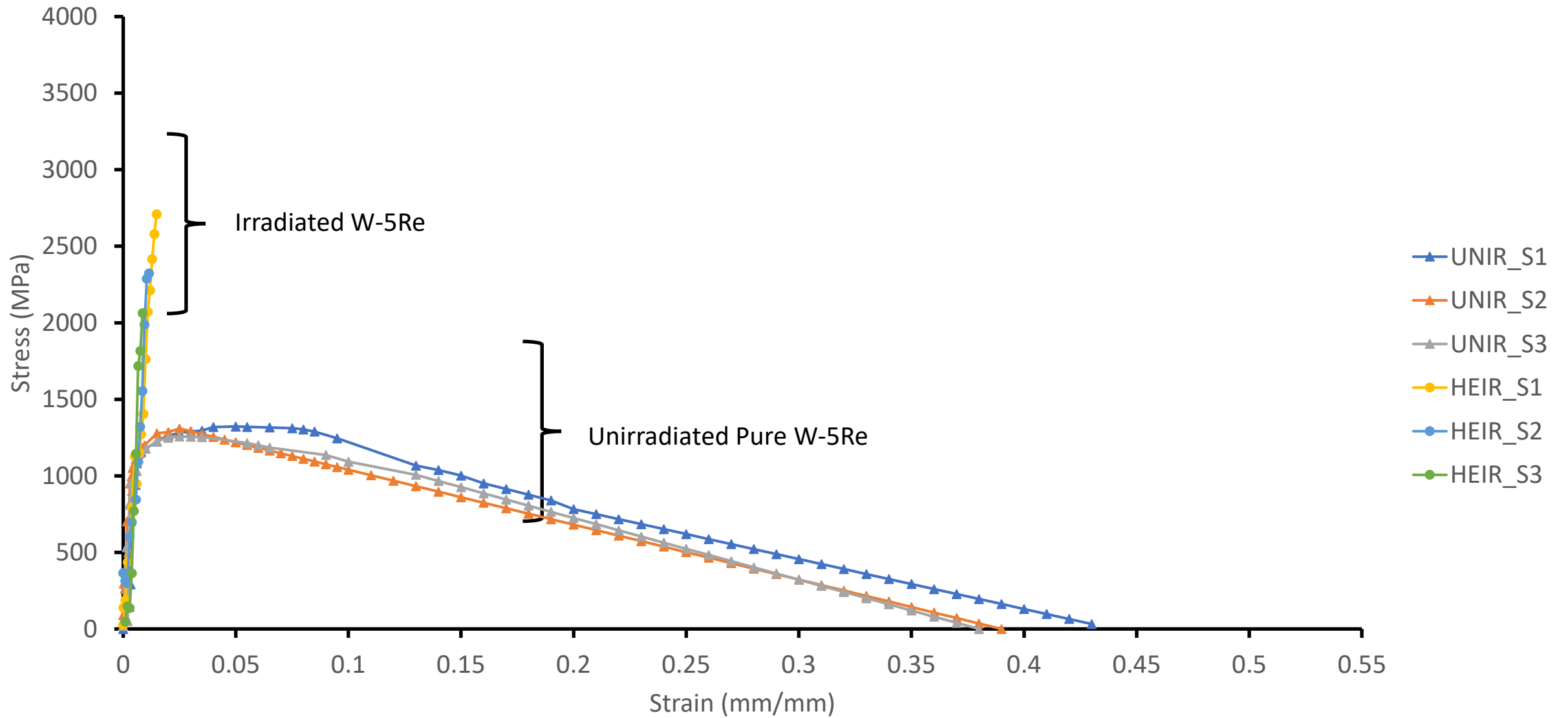


Figure 3(c). Stress-strain plot of micro-tensile samples of W-5Re alloys unirradiated (UNIR) and helium ion irradiated (HEIR).

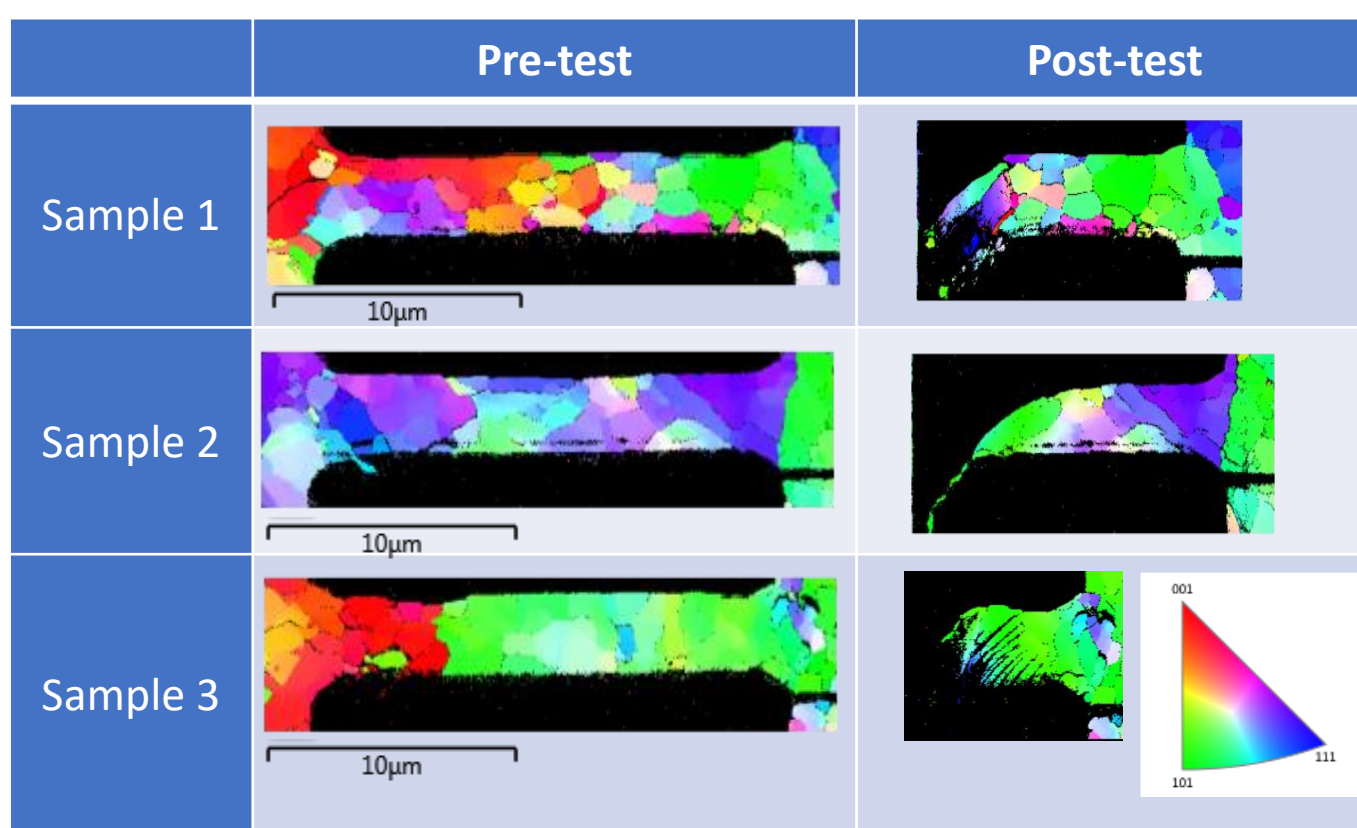


Figure 4 (a). EBSD IPF plots showing grain orientation relative to the tensile axis direction for unirradiated pure W micro-tensile samples.

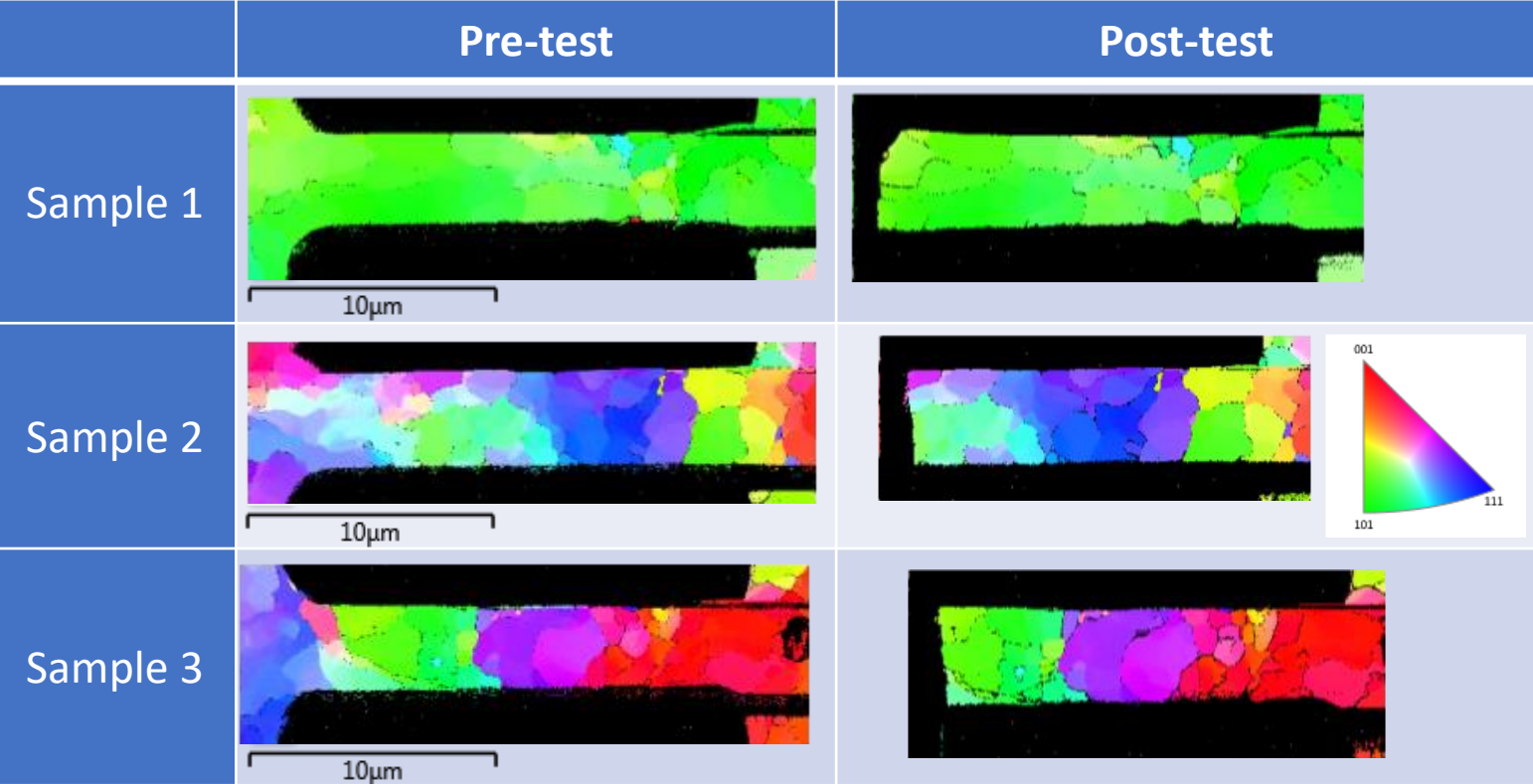


Figure 4 (b). EBSD IPF plots showing grain orientation relative to the tensile axis direction for irradiated pure W micro-tensile samples.

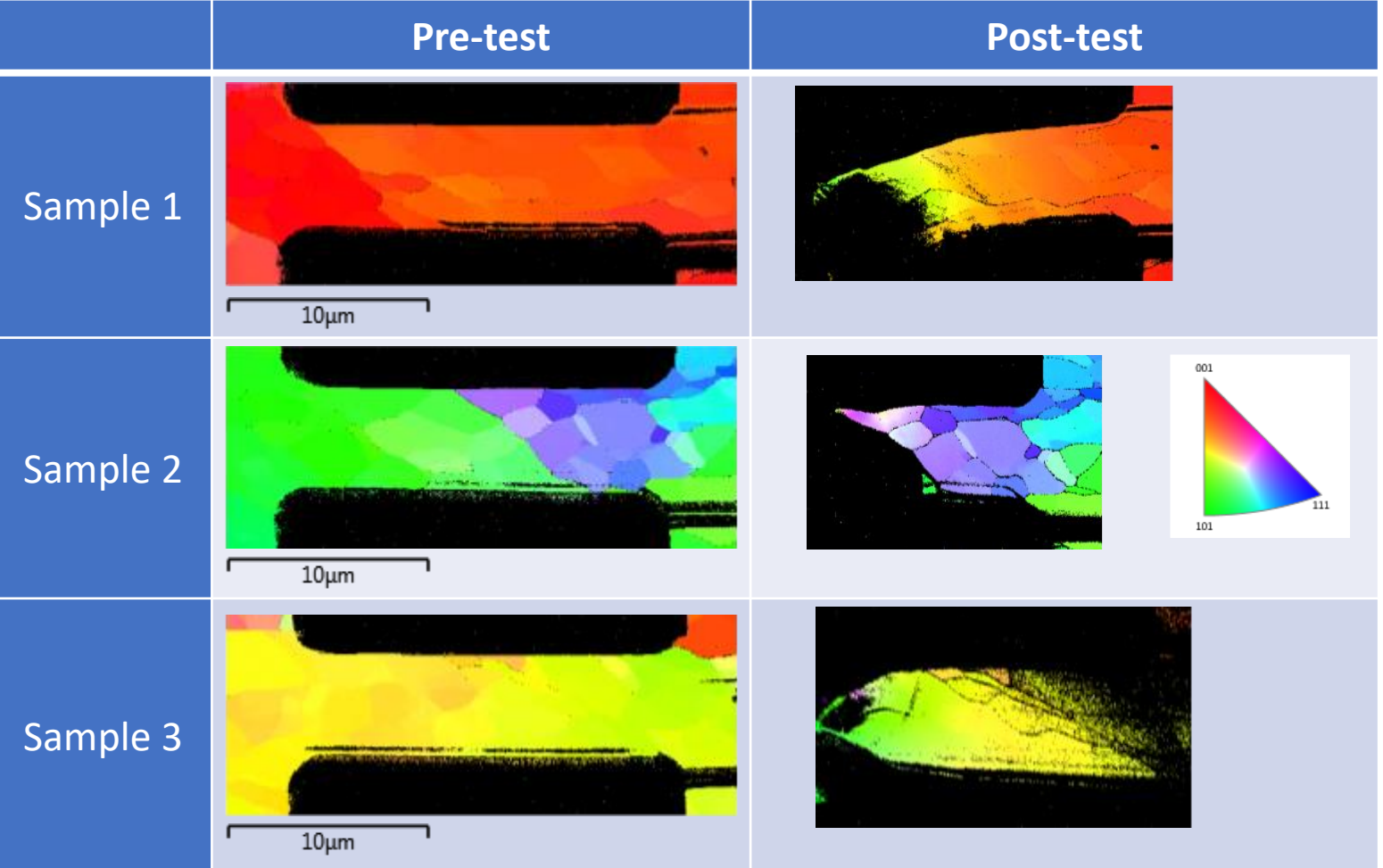


Figure 5 (a). EBSD IPF plots showing grain orientation relative to the tensile axis direction for unirradiated W-5Ta micro-tensile samples.

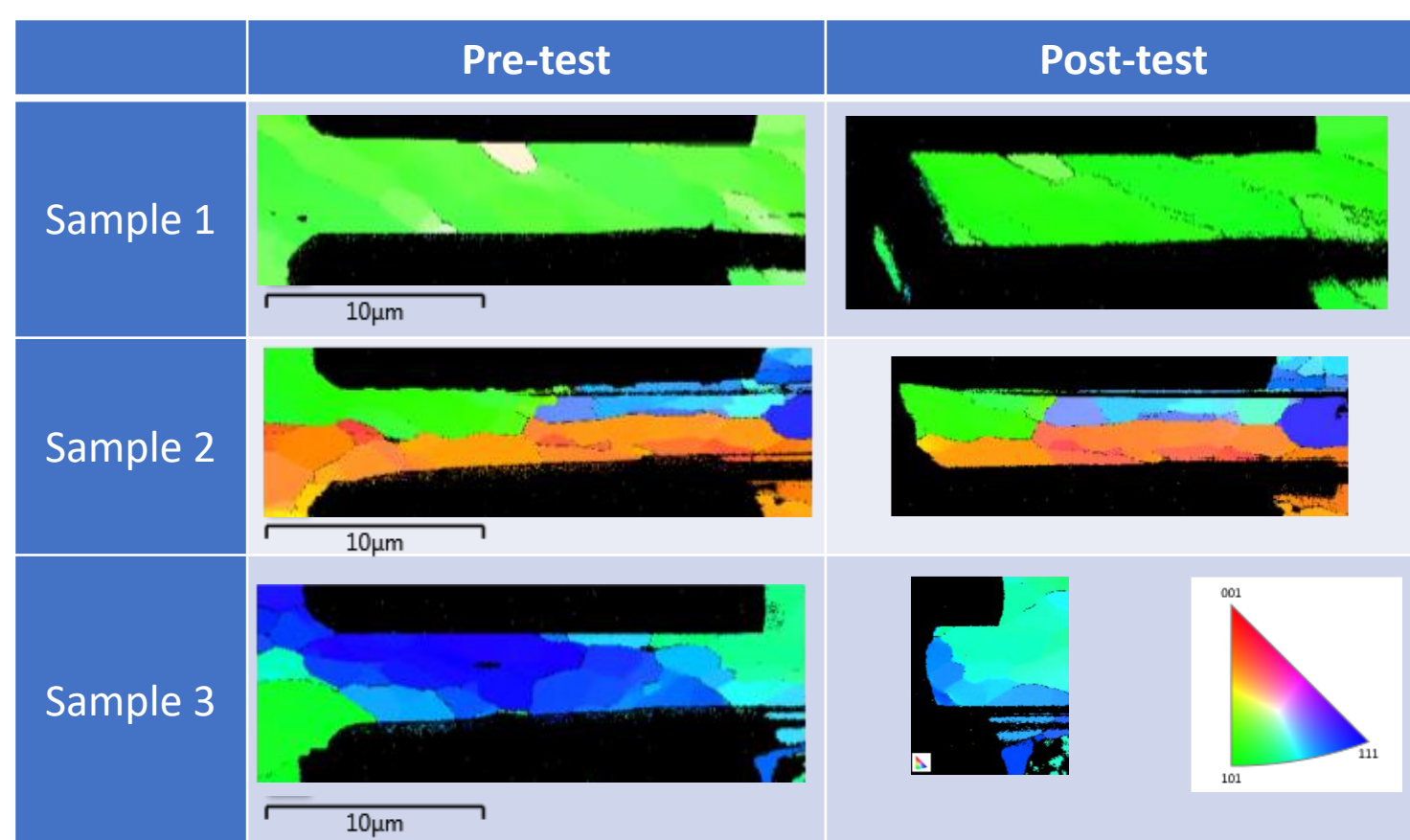


Figure 5 (b). EBSD IPF plots showing grain orientation relative to the tensile axis direction for irradiated W-5Ta micro-tensile samples.

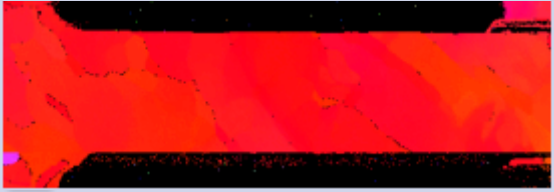
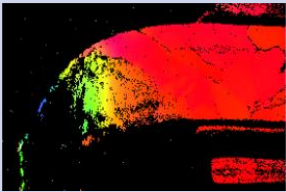

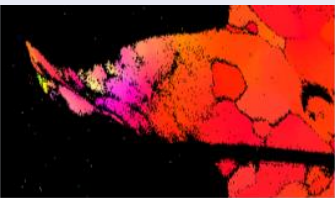
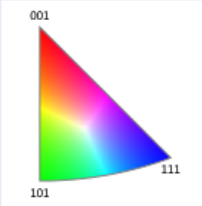
	Pre-test	Post-test
Sample 1		
Sample 2		 

Figure 6 (a). EBSD IPF plots showing grain orientation relative to the tensile axis direction for unirradiated W-5Re micro-tensile samples.

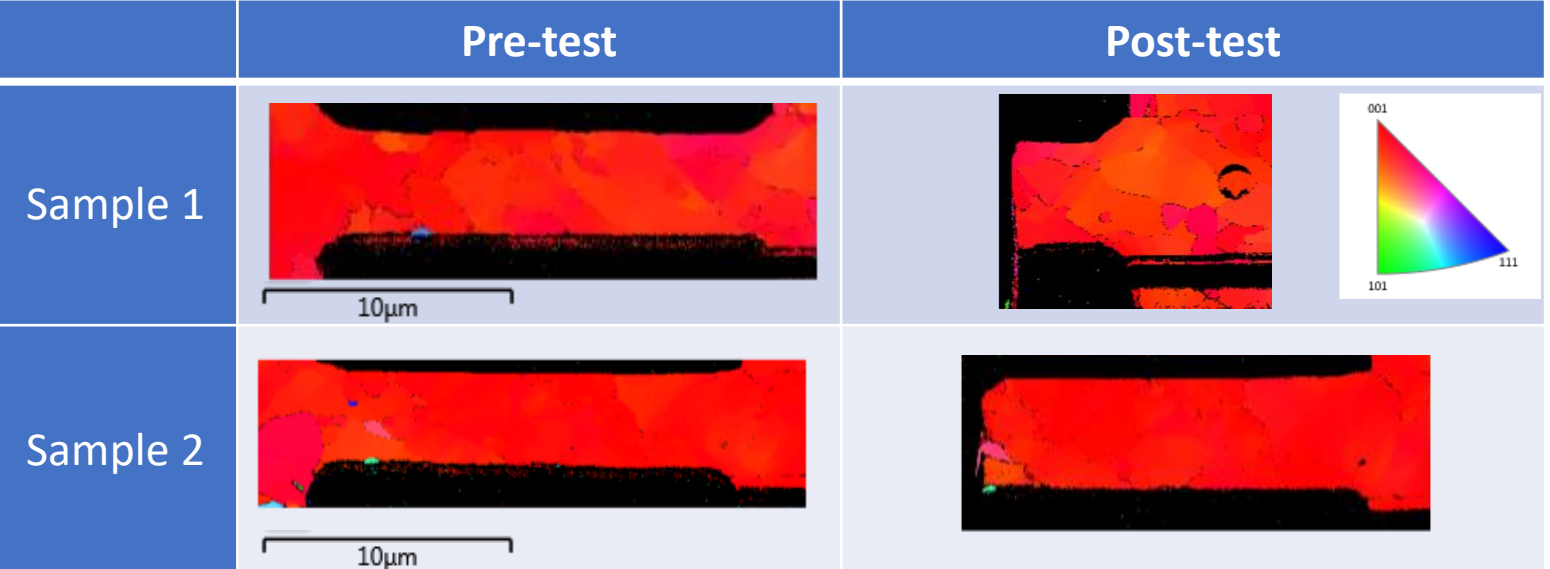


Figure 6 (b). EBSD IPF plots showing grain orientation relative to the tensile axis direction for irradiated W-5Re micro-tensile samples.

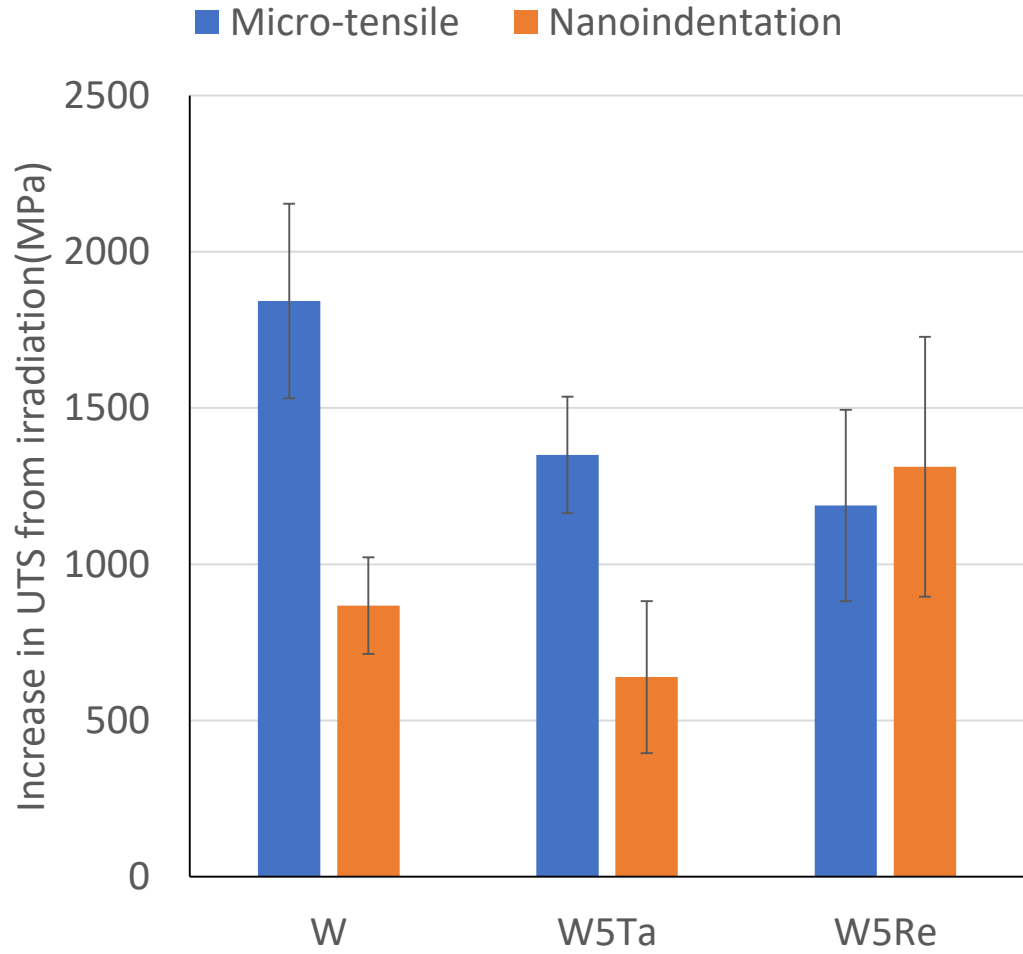


Figure 7. The increase in UTS from irradiation as calculated via micro-tensile and nanoindentation.